JNeurosci
THE JOURNAL OF NEUROSCIENCE

Research Articles | Behavioral/Cognitive

Learning rapidly reshapes brain microstructure: evidence from dense temporal sampling of diffusion MRI

https://doi.org/10.1523/JNEUROSCI.1110-26.2026

Received: 24 June 2026
Revised: 25 September 2026
Accepted: 21 October 2026

Copyright © 2026 the authors

This Early Release article has been peer reviewed and accepted, but has not been through the composition and copyediting processes.The final version may differ slightly in style or formatting and will contain links to any extended data.

Alerts: Sign up at www.jneurosci.org/alerts to receive customized email alerts when the fully formatted version of this article is published.

Learning rapidly reshapes brain microstructure: evidence from dense temporal sampling of diffusion MRI

Running title: Learning rapidly reshapes brain microstructure

Authors: Deniz Kumral[1,2*], Antonia Lenders[1], Monika Schönauer[1,2,3]

Affiliations:

[1]Institute of Psychology, Neuropsychology, University of Freiburg, Freiburg im Breisgau, 79106, Germany

[2]BrainLinks-BrainTools, University of Freiburg, Freiburg im Breisgau, 79106, Germany

[3]Bernstein Center Freiburg, University of Freiburg, Freiburg im Breisgau, 79106, Germany

* D. Kumral, Institute of Psychology, Neuropsychology, University of Freiburg; Freiburg im Breisgau, Germany, Engelbergerstraße 41, Freiburg im Breisgau, 79106, Germany

Email: deniz.kumral@psychologie.uni-freiburg.de

Number of figures: 7
Number of tables (Supplementary): 7
Abstract: 227 words
Significant statement: 97
Introduction: 640 words
Discussion: 1493

Conflict of interest statement: The authors declare no competing financial interests.

Acknowledgments

We would like to express our gratitude to Tobias Debor, who helped with the experimental setup. We also thank all research assistants for helping with data collection.

This project was supported by Deutsche Forschungsgemeinschaft (DFG, German Research Foundation) – Project number: 426865207

JNeurosci Accepted Manuscript

Abstract

Learning is associated with rapid microstructural changes in the human brain, yet the precise temporal dynamics of these changes remain unclear. Using dense temporal sampling of diffusion-weighted MRI (DW-MRI) combined with task-based fMRI, we assessed microstructural changes throughout a declarative learning paradigm and subsequent rest. Seventy-four participants (36 females) learned image-location associations across four encoding-retrieval repetitions while undergoing interleaved functional and DW-MRI acquisitions. A matched control group (N=37, 21 females) underwent a similar imaging protocol without learning. Dense sampling of DW-MRI acquisitions (2146 images across 22 time points in 127 min) revealed that learning-induced mean diffusivity (MD) decreases emerged shortly after learning onset and continued to develop during post-learning rest. The most robust change was localized to the left middle occipital/temporal gyrus, a region also showing functional activation during encoding and retrieval. Linear mixed-effects modeling further confirmed a significant group-by-time interaction, with MD reductions in the left middle occipital/temporal gyrus emerging as early as ≈7 min after learning onset, becoming robust by ≈35-40 min, and persisting throughout the extended post-learning period, while controls showed no changes. Our findings demonstrate that learning-related microstructural plasticity unfolds continuously from encoding to offline consolidation, with learning-induced structural changes emerging in functionally engaged regions. Dense temporal sampling of DW-MRI offers a powerful approach to bridge functional activation and structural remodeling, providing evidence of *when* and *where* experience-dependent plasticity occurs during memory formation.

JNeurosci Accepted Manuscript

Significance Statement

How quickly does the brain's structure change when we learn? Using dense temporal sampling of diffusion-weighted MRI (DW-MRI; 2146 images) across more than 2 hours, we show that microstructural plasticity arises rapidly during learning and continues to develop during post-learning rest. These learning-induced changes are spatially precise and overlap with task-related functional activity. By capturing the entire progression of microstructural plasticity across the learning process, rather than just before and after a learning paradigm, our study provides insights into *when* and *where* learning-induced plasticity occurs, demonstrating that memory formation involves rapid, ongoing microstructural changes in functionally engaged regions.

JNeurosci Accepted Manuscript

Introduction

Learning induces not only transient functional changes in the brain, but also enduring structural modifications that support memory functions. Classic theories of systems consolidation propose that new experiences are first encoded by hippocampal–medial temporal circuits and then gradually integrated into distributed neocortical networks (McClelland et al., 1995; Frankland and Bontempi, 2005; Brodt and Gais, 2021). Traditionally, this process was thought to unfold slowly, requiring extended offline reactivation and reorganization (Klinzing et al., 2019). However, recent neuroimaging studies have indicated that microstructural remodeling can emerge within hours of a new experience (Sagi et al., 2012; Brodt et al., 2018; Tavor et al., 2020; Friedman et al., 2025), raising the question of *when the first* learning-induced microstructural changes can be observed in the human brain.

MRI has become central to assessing learning-induced changes at both the functional and structural levels. Functional MRI (fMRI), through the blood oxygenation level–dependent (BOLD) signal, has been used extensively to map the regions engaged in learning and memory (Brodt et al., 2016). However, while fMRI captures the hemodynamic correlates of neural activity, it does not reveal whether these regions undergo concurrent structural changes. Conversely, structural MRI (e.g., T1-weighted) has traditionally focused on long-term changes in gray matter volume (i.e., voxel-based morphometry) or cortical thickness accompanying extended training (Draganski et al., 2004; Zatorre et al., 2012; Hebscher et al., 2019; Kleinschroth et al., 2026). While these macroscopic changes are informative, they provide little insight into the microstructural processes occurring over shorter timescales.

Diffusion-weighted MRI (DW-MRI) provides an indirect measure of brain microstructure by assessing how freely water molecules move through tissue (Bihan, 1995, 2012). Mean diffusivity (MD), measuring the diffusive motion of water molecules, is particularly sensitive to microstructural changes (Assaf et al., 2019). Decreases in MD have been observed within hours of learning, including spatial navigation (Sagi et al., 2012; Tavor et al., 2013; Keller and

JNeurosci Accepted Manuscript

Just, 2016), language learning (Hofstetter et al., 2017), and associative memory (Brodt et al., 2018), as well as motor learning (Jacobacci et al., 2020; Callow et al., 2023; Stee et al., 2023; Griffa et al., 2024; Friedman et al., 2025), and are thought to reflect processes such as synaptic changes, astrocyte functioning, and the expression of brain-derived neurotrophic factor (Johansen-Berg et al., 2012; Sagi et al., 2012), which is a marker for long-term potentiation. Although the aforementioned studies have demonstrated that learning induces microstructural changes in the human brain, the vast majority of research, including our own (Brodt et al., 2018), have used pre-post designs that cannot capture the temporal dynamics of plasticity (Villa et al., 2026). In contrast, continuous diffusion acquisition strategies, such as moving-average or sliding-window approaches, indicate that diffusion metrics can change within minutes (Darquié et al., 2001; Friedman et al., 2025). These findings suggest that learning-related plasticity is rapid and temporally heterogeneous across the brain. Nevertheless, it remains unclear whether these temporal dynamics extend to declarative memory. Specifically, do microstructural changes arise concurrently with learning, accumulate gradually across practice, or emerge only later, after learning has ended? How, *when*, and *where* are these changes stabilized in the brain?

In the present study, using dense temporal sampling of DW-MRI, we aimed to determine the spatiotemporal dynamics of learning-induced plasticity in humans, identifying *where* and *when* human brain microstructural plasticity arises. To investigate our aim, participants performed an image-location learning task which measures associative memory while undergoing an imaging protocol that interleaved traditional task-based fMRI runs with DW-MRI acquisitions. Following the task, participants underwent repeated DW-MRI acquisitions, allowing us to assess whether microstructural plasticity extended into the immediate post-learning phase. Crucially, the dense sampling of DW-MRI was designed to sensitively assess microstructural changes as they emerge and evolve throughout learning and post-learning rest phase. Rather than relying on pre-post comparisons, this design allowed us to determine when and where learning-induced microstructural changes emerge in functionally engaged regions.

JNeurosci Accepted Manuscript

Materials and Methods

Participants. Participants were recruited via the SONA online recruitment system, email, flyers, posters, and online advertisements. Potential participants were screened for eligibility through structured phone interviews. Eligible participants were between 18 and 35 years of age and were native German speakers or demonstrated at least B2-level proficiency in German. The exclusion criteria were current or previous treatment for psychological disorders, history of neurological conditions, untreated visual impairments, and contraindications for MRI. A total of 125 eligible participants were recruited, with 84 assigned to the learning condition and 41 to the control condition. Participants were excluded due to incidental findings (n = 2), falling asleep during data acquisition (n = 1), or withdrawing due to discomfort in MRI (n = 4; including 2 from the control group), resulting in an initial sample of 118 individuals: 79 in the learning group (*M* = 23.32 ± 2.96 years of age; 39 female) and 39 in the control group (*M* = 24.82 ± 3.50 years of age; 21 female). Additional exclusions were made due to poor image alignment (n = 3), excessive motion (mean framewise displacement averaged across sessions > 0.6 mm; n = 2), or incomplete datasets (n = 3). The final sample included 74 participants in the learning group (*M* = 23.22 ± 2.93 years; 36 females) and 37 in the control group (*M* = 24.70 ± 3.48 years; 21 females).

Participants were compensated at a rate of €10/hour for behavioral sessions and €15/hour for neuroimaging sessions, with total reimbursement ranging from €40 to €70, depending on the total time spent in the experiment. The study was conducted in accordance with the Declaration of Helsinki and approved by the local ethics committee (approval number: 21-1553) and all participants provided written informed consent. All tests were performed at the Department of Radiology, University Medical Center Freiburg, Germany.

Experimental Procedure. Upon arrival, the participants received an MRI safety briefing and detailed instructions regarding the study procedure. They then completed a short tutorial of the image-location task and were randomly assigned to scanning group A, starting with fMRI acquisition during the first rehearsal block (N=37 in learning, N=18 in control), or B, starting

JNeurosci Accepted Manuscript

with DW-MRI acquisition during the first rehearsal block (N=37 in learning, N=19 in control; see **Fig. 1**). The experimental session began with baseline acquisitions, including T1-weighted, T2-weighted, and DW-MRI (N_{acq} =2) anatomical scans. In the learning group, after the baseline scans were measured, individuals completed N-back tasks, which serve as a localizer. This was followed by four repetitions of the image-location task, where task-based fMRI (N_{acq} = 2) and DW-MRI (N_{acq} =8) were interleaved throughout the task (**Fig. 1**). After completing the image-location task, participants had a brief break before continuing the post-learning phase, which comprised resting-state fMRI (N_{acq} =2) and DW-MRIs (N_{acq}=12), followed by a final T1-weighted MRI. The final (fifth) retrieval session was conducted outside the MRI.

The imaging procedure for the control group was largely equivalent to that of the experimental group. However, instead of performing the memory task, participants remained at rest during the phase when the task occurred for the learning group. Resting-state fMRI and DW-MRIs were acquired in an interleaved fashion following baseline imaging (N_{acq} =2). After this phase, participants had a 90-min break and were instructed to avoid eating a full meal, studying, watching videos, exercising, or sleeping. Following the break, they returned to the MRI for the final session, which included four DW-MRI and T1-weighted MRI acquisitions.

Image Location Task. During the experiment, participants were required to encode and recall item-location associations (Brodt et al., 2018). The experiment consisted of four encoding-retrieval repetitions and one additional post-scan behavioral retrieval session. During encoding, participants viewed 28 image pairs presented in random order. Each image was assigned a unique location on a 7×4 grid. The first image was shown full screen for 1.5 s to ensure that participants could perceive all visual details, then was moved onto its grid location in a continuous animation over 1 s, and remained visible there for 3 s. The second image (target) was then presented with the same durations; during the zoom-in period of the second image, the first image remained visible at its grid location, but was removed once the second

JNeurosci Accepted Manuscript

image reached its position, such that the two images were not displayed together on the grid at the end of the trial (**Fig. 2).** The inter-trial intervals ranged from 1.7 to 2 s. Each image appeared in two different pairs, once as the first item and once as the second item. In the cued retrieval phase, the first image of each pair was presented for 2.5 s full screen before moving to its location on the grid. Participants navigated the grid using two button boxes (index and middle fingers of both hands for up, down, left, and right movements), with a red frame indicating the current position. Confirmation of the second image's location was made by pressing a separate button with the pinky finger, turning the red frame white. The participants then used a red cursor to indicate the location of the second image. Confirmation was made by pressing a separate button. Each trial lasted up to 11.5 s, after which the cursor's position was automatically recorded. All 28 pairs were tested once per retrieval session in a randomized order. At pseudorandom intervals, participants completed an active baseline task, classifying digits (1-9) as odd or even within a 2-sec response opportunity (Stark and Squire, 2001). Each baseline period lasted ~7.5 s, and digits were not repeated consecutively. The task was programmed using PsychoPy 2022.2.4 and was projected onto an MRI-compatible screen at the back of the scanner bore and viewed by participants via a mirror attached to the head coil. After scanning, the participants completed a fifth retrieval run on a desktop computer, again identifying the second-image locations.

MRI Acquisition. Brain imaging was performed on a 3T PRISMA MRI scanner (Siemens Medical Systems, Erlangen, Germany) with a standard 64-channel head coil at the University of Freiburg, Medizinisch Klinik, Hugstetterstraße 55, 79106, Freiburg, Germany. To minimize offline warping, an auto-alignment scout was used to automatically position the measurement volumes consistently across baseline and post-learning scans.

Structural images were recorded with T1-weighted 3D high-resolution structural MRI brain scans (baseline and post-learning) using a GRAPPA sequence (acceleration factor 2) with the following parameters: TR = 2300 ms, TE = 4.18 ms, TI = 900 ms, slice thickness = 1.0 mm,

JNeurosci Accepted Manuscript

bandwidth = 150Hz/Px, FA = 9°, FOV = 256 mm, and voxel size = 1.0 × 1.0 × 1.0 mm^3, with 176 slices collected for a total collection time of 5:30 min. Likewise, we measured T2-w 3D high-resolution structural scans using a GRAPPA sequence (acceleration factor 2) with TR = 3200.00 ms, TE = 564.00ms, FA1 = 90º, FA2 = 120º, slice thickness = 0.8 mm, FOV = 256 mm, bandwidth 744Hz/Px, with a voxel size 0.8 x 0.8 x 0.8 mm^3; 208 slices collected for a total collection time of 5:57 min.

The functional images were acquired via an echo-planar sequence (EPI) using the following parameters: TR = 1750 ms, TE = 30 ms, FA = 68°, FOV = 220 mm, imaging matrix = 88 × 88, with voxel size = 2.5 x 2.5 × 2.5 mm^3, slice thickness = 2.5 mm, echo spacing = 0.52 ms, bandwidth = 2272 Hz/Px, 69 slices with an interleaved slice acquisition. A gradient echo field map with the sample geometry was used for distortion correction (TR = 400 ms, TE 1 = 4.92 ms, TE 2 = 7.38 ms, FOV = 205 mm, slice thickness = 3.2 mm). Imaging data were organized according to the Brain Imaging Data Structure (BIDS; Gorgolewski et al., 2016) to standardize data storage and allow for the application of automatic preprocessing pipelines.

DW-MRI scans were obtained with b-values 0 - 1000 s/mm^2, in 30 whole-sphere gradient directions; 6 interspersed b0 images; TR = 2500.00 ms, TE = 53.00 ms, FOV = 220 mm, voxel size 2.5 x 2.5 x 2.5 mm^3, partial Fourier ⅞, slice thickness 2.5 mm with 56 slices with a total time of 1:55 min (Brodt et al., 2018). To enable use of FSL's (Jenkinson et al., 2012) distortion correction tools topup and eddy, we acquired consecutively anterior-to-posterior and posterior-to-anterior phase encoding directions, totaling 44 DW-MR images (4 baseline, 16 learning, 24 post-learning) for learning and 28 DW-MR images (4 baseline, 16 learning rest, 8 post-learning) for the control group.

Structural and Functional MRI Data Preprocessing. Anatomical and fMRI data were converted to BIDS format (Gorgolewski et al., 2016) and later preprocessed using fMRIPrep 21.0.1 (Esteban et al., 2020) and Nipype (Gorgolewski et al., 2011). Briefly, the T1-weighted images were corrected for intensity non-uniformity, skull-

JNeurosci Accepted Manuscript

stripped, and spatially normalized to MNI152NLin2009cAsym space using advanced normalization tools (ANTs; Avants et al., 2011). For functional data, we applied slice-timing correction and head-motion correction with six degrees of freedom. The BOLD data were co-registered to T1-weighted images, and nuisance regressors (e.g., framewise displacement [FD], DVARS, and CompCor) were computed. Finally, the BOLD time-series were spatially normalized to standard space using ANTs. Additional preprocessing was performed using Python code that included removal of 4 volumes of each image and also spatial smoothing with a 6 mm full-width at half-maximum (FWHM) Gaussian kernel.

DW-MRI Data Preprocessing. Preprocessing of DW-MRI involved motion and eddy-current distortion correction using FSL's *topup* and *eddy*. For each time point, all images across the two phase-encoding directions (1 AP, 1 PA) were combined, resulting in 22 DW-MRIs in the learning and 14 DW-MRIs in the control group. Tensor calculation was performed using FSL's *dtifit*, based on eddy-rotated b-vectors (Basser et al., 1994). Because fractional anisotropy (FA) images contain more structural landmarks, the registration was estimated on the FA data. Each participant's FA image was co-registered to their high-resolution T1-weighted anatomical image (from *fMRIPrep*) using a 6 degrees-of-freedom linear registration (FSL *flirt*). This FA-to-T1 transform was then concatenated with the fMRIPrep-derived T1-to-MNI transform (MNI152NLin2009cAsym), and the combined transformation was applied to the MD images in a single resampling step using *antsApplyTransforms*. After registration, the MD images were smoothed using a 6 mm FWHM Gaussian kernel. This kernel was selected based on the approach used in previous DW-MRI work on rapid learning-related microstructural changes (Brodt et al., 2018; Stee et al., 2023) and to match the spatial smoothing applied to the fMRI data, thereby maintaining a comparable spatial scale across modalities.

Statistical Analyses

JNeurosci Accepted Manuscript

Memory Performance in the Image-Location Task. Behavioral performance was quantified using i) the percentage of correctly recalled locations of the paired images and ii) a normalized Manhattan distance, defined as the response-to-target distance (horizontal and vertical steps) divided by the start-to-target distance, such that values <1 reflect movement toward and values >1 reflect movement away from the correct location. To assess whether participants improved their memory performance over learning repetitions, we applied a within-subject repeated-measures ANOVA. To compare performance at the fourth and fifth retrieval sessions against the first, we conducted paired-samples *t*-tests. All tests were two-tailed with an α level of 0.05. Due to incomplete data, one participant was excluded from both the behavioral and fMRI analyses.

Univariate fMRI Analyses. Functional data were analyzed using SPM12 (Wellcome Department of Cognitive Neurology, London, UK, https://www.fil.ion.ucl.ac.uk/spm). The preprocessed BOLD time series were high-pass filtered with a 128 s cutoff. A two-level general linear model (GLM) approach was used. First-level analyses were conducted using fixed effects at the individual level. The conditions of interest, encoding, recall, and baseline, were modeled for each repetition. The encoding time was defined as lasting from the onset of the first item of the image pair to the offset of the second item, while retrieval trials were specified as the duration from the onset of the first item to one volume before the participant made their first cursor movement, thus reducing motion-induced noise. If participants did not move the cursor, a time limit of 11.5 seconds was used as the offset of the retrieval event. The baseline time was defined as the onset and offset of the odd-even task. BOLD responses were modeled by convolving the event timings with the canonical hemodynamic response function. Six motion parameters were included as nuisance regressors.

We spatially smoothed the first-level contrast images, baseline-subtracted per condition, with an 8 mm FWHM Gaussian kernel before entering them into the second-level analysis. Full factorial models were computed with the factors of repetition and scanning groups. To

JNeurosci Accepted Manuscript

preserve statistical power across runs, all trials, regardless of retrieval accuracy, were included. For second-level analyses, we used a linear contrast across runs (+1 +1 +1 +1) to assess the general activity during encoding and retrieval. Significant results were reported following family-wise error (FWE) correction for multiple comparisons (p_{FWE}<.05, k=20 voxels).

DW-MRI Group-level Analyses. To assess group-level microstructural changes, flexible factorial models were used with time, experimental groups, scanning groups, and individuals as factors applied to whole-brain MD analyses in the MNI space. A total of 2146 images were included in the model. For the learning group, a linear decrease contrast was defined across all 22 acquired sessions using monotonically decreasing weights ranging from +11 to −11. For the control contrast, weights were constructed to temporally align with the corresponding time points in the learning group. This strategy ensured that, at each contrast, the full available sample in both groups contributed to the estimation while preserving temporal correspondence between groups despite unequal acquisition timings. Based on these group-specific vectors, a group × time interaction contrast was computed by directly contrasting the learning-related decrease with the corresponding timing-matched control condition (learning > control). Significant results were reported according to the FWE correction at the voxel level for multiple comparisons (p_{FWE}<.05, k=20 voxels). To control for differences in the field of view, a whole-brain mask including gray matter, white matter, and cerebral spinal fluid (CSF) was created for each participant and session by excluding voxels deviating more than ±1 SD, and this mask was applied to the group-level analyses. Thus, the group-level analysis was performed across the whole brain rather than being restricted a *priori* to gray matter. Significant clusters were anatomically localized using the Harvard–Oxford cortical and subcortical probabilistic atlases implemented in FSL (Jenkinson et al., 2012).

To confirm that our findings did not depend on the choice of smoothing kernel, we also smoothed the DW-MRI data using a Gaussian kernel with a FWHM of 3 mm (approximately 1.25 times the voxel size) instead of the 6 mm kernel used in the primary analyses and repeated the whole-brain flexible factorial analysis, described above.

JNeurosci Accepted Manuscript

To further explore the temporal trajectories of learning-induced MD changes across the whole brain, we contrasted the MD change from baseline (t_1) to each subsequent time point ($t_{2\text{-}22}$) against the corresponding change in the control condition. This was implemented as an interaction contrast (i.e., [learning_t_n − learning_t_1] - [control_t_n − control_t_1]), resulting in 21 comparisons ($p_{uncorrected}$<.001, k=20 voxels). For these contrasts, the corresponding control scans were defined by using temporally corresponding session(s). For time points of t_{11}-t_{19}, where no temporally matching control sessions were available, the final DW-MRI acquisition (t_{10}) during the learning interval was used. By subtracting the control-related change from the learning-related change, these contrasts isolate MD changes specific to learning while accounting for nonspecific temporal effects.

To quantify the spatial consistency of learning-dependent MD changes over time, we performed a voxelwise overlap analysis across these 20 statistical maps, starting from learning onset (t_3) for all subsequently sampled timepoints (t_3-t_{22}). Each map was binarized, and the resulting binary maps were summed voxel-wise to generate an overlap count image indicating the number of maps in which each voxel was present. An overlapping cluster was then derived by thresholding the overlap count at ≥10 maps (i.e., presence in at least 50% of all contrasts).

To determine whether the overlapping cluster (i.e., left middle occipital/temporal gyrus) coincided with functional activity during encoding and retrieval, we used joint inference analyses. First, the DW-MRI image was downsampled to the spatial resolution of the fMRI (2.5 mm). We then binarized the thresholded encoding and retrieval statistical maps (p_{FWE}<.05, k=20 voxels) by retaining voxels with values greater than zero. A conjunction map was computed by taking the voxel-wise logical AND across the three binarized maps, identifying voxels that were jointly present in the encoding, retrieval, and left middle occipital/temporal gyrus.

Analysis of fractional anisotropy. To further examine whether the pattern of learning-related microstructural changes extended to tissue anisotropy, we additionally extracted FA images

JNeurosci Accepted Manuscript

from the same *dtifit* tensor fits used to derive MD and repeated the group-level flexible factorial analysis on FA maps. Based on prior evidence of learning-related FA increases (Scholz et al., 2009; Sagi et al., 2012), the interaction contrast tested for FA increases in the learning group relative to controls. The same whole-brain mask, statistical thresholds (p_{FWE}<.05, k=20 voxels), and temporal overlap analysis described above for MD were applied to the FA data. Significant clusters were anatomically characterized using the Harvard Oxford Atlas together with JHU ICBM-DTI-81 White-Matter Labels and JHU White-Matter Tractography atlases (Hua et al., 2008; Mori et al., 2008) .

Linear Mixed-effects Model. To test for time-resolved MD changes between learning and control conditions, we next used linear mixed models using the *lme4* package (Bates et al., 2015) in R (version 4.3.1; R Core Team, 2023) with individuals as a random effect. We first extracted the MD values from the left middle occipital/temporal gyrus (k=17 voxels) across 22 DW-MRI scans (group A and B) acquired for each participant, capturing 38 distinct time points across the experimental protocol spanning ≈127 min, representing the real acquisition times rather than acquisition indices. These time points included baseline measurements (t_1-t_2, <20 min), learning task periods (t_3-t_{18}, 0-61 min), and an extended post-learning rest phase (t_{19}-t_{38}, ≈74-127 min), allowing for a comprehensive characterization of the temporal dynamics in the brain microstructure.

We used two models to enable targeted testing of the group-by-time interaction effect.

1. The null model included the main effects of time (as a factor with 38 levels representing different measurement time points across the baseline, task, and post-task periods) and group (learning vs. control), along with the scan group (A vs. B). A random intercept for participant ID was included to account for repeated measurements within individuals.
2. The full model was identical to the null model, except for the addition of the group-by-time interaction term, which represented the effect of primary interest (group × time).

JNeurosci Accepted Manuscript

3. The difference between the full and null models was tested using the anova function and setting the argument test to the chi-square (χ^2) test. Statistical significance was set at $\alpha = 0.05$.
4. In the case of significant interactions, the effects at the individual levels of predictors were analyzed post-hoc using Holm correction from the *emmeans* package (Lenth and Piaskowski, 2017). Note that we were only interested in examining MD changes from baseline within each group separately. For each group, we compared all time points ($t_{2\text{-}38}$) to the baseline (t_1) using the *contrast*() function with the "trt.vs.ctrl" method.

Association between Memory Performance and Microstructural Plasticity. We performed two different correlation analyses to assess the correlation between MD and behavioral performance. A repeated-measure correlation (Bakdash and Marusich, 2017) was used to assess whether changes in MD across repetitions during learning were associated with improvements in memory retrieval during learning. Given the design with two scanning groups (Group A, $N = 36$: 1st and 3rd retrieval; Group B, $N = 37$: 2nd and 4th retrieval), analyses were performed at the two relevant time points per participant, and participant-specific mean MD values were extracted. We then averaged the MD values separately for each participant based on repetition, grouping runs 1 and 3 (A) and runs 2 and 4 (B), corresponding to their respective retrieval sessions. Repeated-measure correlations were then conducted using the *rmcorr* package in R (Bakdash and Marusich, 2017), which accounts for within-subject dependencies in the data and ensures robustness to potential violations of normality and homogeneity of variance. To further investigate brain-behavior relationships, Pearson's correlation was used to test whether microstructural plasticity was related to memory gain. Microstructural change was defined as the percentage change in MD between the baseline (t_1) and post-learning session (t_{22}), and behavioral change as the improvement in recall (percentage and Manhattan Distance) between the first and fifth repetitions. All statistical analyses were performed using R (version 4.3.1; R Core Team, 2023).

JNeurosci Accepted Manuscript

Results

Behavioral Performance. The repeated-measures ANOVA revealed a significant main effect of repetition on memory performance ($F(4, 353) = 45.54$, $p < .001$, $\eta 2 = .37$ for percentage and $F(4, 353) = 35.75$, $p < .001$, $\eta 2 = 0.33$ for normalized Manhattan Distance, **Fig. 3B**). Post-hoc paired t-test comparisons showed that the percentage of correct answers significantly increased from the first ($M = 15.11$, SD = 10.94) to the fourth ($M = 67.66$, SD = 29.80) retrieval run ($t(72) = -17.03$, $p < .001$), and also from the first to the fifth retrieval ($M = 63.83$, SD = 30.2, $t(70) = -15.51$, $p < 0.001$**; Fig. 3A**). Likewise, we observed that the normalized Manhattan Distance decreased from the first ($M = 1.15$, SD = 2.81) to the fourth ($M = 0.42$, SD = 0.42) retrieval run ($t(72) = 16.038$, $p < 0.001$; **Fig. 3B**) and also from the first to the fifth retrieval ($M = 0.473$, SD = 0.429, $t(70) = 15.025$, $p < 0.001$). As expected, participants improved in recalling the items of an image-pair and their respective locations over learning repetitions.

fMRI Activity during Encoding and Retrieval. We conducted whole-brain analyses to identify brain regions associated with general functional activity changes during encoding and retrieval phases compared to an odd-even number judgement task. We observed widespread areas, including the occipital cortex extending to the temporal, parietal, and prefrontal cortices ($p_{FWE}<.05$, k=20 voxels, **Fig. 3C**; Table S1-S2).

Learning-related Microstructural Changes in MD. We first defined a linear decrease contrast across all 22 acquired sessions using a whole-brain flexible factorial analysis with a group × time interaction, comparing the learning group against the control group. This revealed learning-specific decreases in MD (relative to control) in several brain regions, including the superior occipital gyrus, precuneus, cuneal cortex, superior parietal lobule, postcentral gyrus, cerebellum, middle occipital/temporal gyrus, and angular gyrus (**Fig. 4**, Table S3). When applying a Gaussian smoothing kernel with a FWHM of 3 mm instead of 6 mm, our findings closely replicated the results of the primary analyses. Similar to our main analyses, a whole-

JNeurosci Accepted Manuscript

brain flexible factorial analysis with a group × time interaction revealed learning-specific decreases in MD in similar brain regions (**Fig. S1**).

We further assessed the temporal trajectories of learning-induced microstructural plasticity by contrasting the MD change from baseline (t_1) to each subsequent time point (t_2-t_{22}) against the corresponding change in the control condition. As expected, at the baseline, no MD changes were detected (t_2). During early learning, effects in the brain were sparse and mostly transient. From approximately the ninth session (t_9), a cluster centred on the left middle occipital/temporal gyrus, falling within the cluster identified in the overall linear-decrease analysis (**Fig. 4**, Table S3), emerged and persisted (**Fig. 5**). Beginning in the post-learning phase (t_{11}), we observed MD decrease in several clusters, which increased steadily in both spatial extent and magnitude, peaking at the final acquisitions (t_{19}-t_{21}). These post-learning effects were predominantly posterior, encompassing the superior lateral occipital cortex, precuneus, and superior parietal lobule. Detailed statistics for the significant clusters of each contrast are provided in Table S4.

To evaluate the robustness of the observed effects, we assessed the spatial consistency of learning-dependent MD changes by overlaying the 20 thresholded contrast images spanning from learning onset to the end of the post-learning period (t_3-t_{22}) and computing their overlap, identifying voxels that showed MD reduction consistently across contrasts. Voxels surviving threshold in at least half of the maps (≥10/20) were retained, yielding a criterion that isolates regions reliably decreased across the time course. This analysis revealed a single robust cluster in the left middle occipital/temporal gyrus (k=17 voxels; peak MNI coordinate [−41, −72, 21]). The cluster was consistently represented from the ninth (t_9) to the twenty-first session (t_{21}), indicating a spatially coherent and temporally stable locus of rapid MD reduction that emerged during the second half of the learning phase and persisted until the end of the measurement, 2 hours after learning onset (**Fig. 5**). Joint inference analysis with fMRI further showed that the left middle occipital/temporal gyrus was activated during both encoding and retrieval (k=14 voxels, [x=-41, y=-72, z=21], **Figure 3D**).

Neurosci Accepted Manuscript

Fine-grained Temporal Dynamics of Microstructural Changes. To characterize how learning-induced microstructural changes in the left middle occipital/temporal gyrus unfolded over time, we applied linear mixed-effects models based on the real acquisition timings rather than acquisition indices. We observed a significant group-by-time interaction effect ($\chi^2 = 59.33$, df = 21, $p < 0.001$), indicating that the temporal trajectories of changes in brain microstructure differed significantly between the learning and control groups. The likelihood ratio test comparing the full model to the null model confirmed that the interaction term significantly improved the model fit ($\chi^2 = 58.49$, df = 21, $p < 0.001$; AIC full model = -44,823 vs. null model = -44,806). Type III Wald chi-square tests further revealed significant main effects of time ($\chi^2 = 94.77$, $p < 0.001$) and group ($\chi^2 = 4.99$, $p = 0.025$), while the scan group (A or B) showed no significant effect ($\chi^2 = 0.02$, $p = 0.886$).

To assess MD differences from baseline to the last session, we used post-hoc analyses, examining MD changes separately for each group **(Fig. 6**). While we observed no significant MD differences at any time in the control group (all $p > 0.05$, with effect sizes ranging from -1.87×10^{-6} to 4.67×10^{-6}), the learning group exhibited significant decreases in MD from baseline across the early task and post-learning rest periods. During the early task phase, the learning group showed small but significant decreases, beginning at ≈7 min ($\beta = -4.67 \times 10^{-6}$, $p = 0.002$) and continuing at 11.5 min ($\beta = -3.41 \times 10^{-6}$, $p = 0.046$), ≈20 min ($\beta = -4.33 \times 10^{-6}$, $p = 0.005$), ≈24 min ($\beta = -3.52 \times 10^{-6}$, $p = 0.039$), and ≈28 min ($\beta = -3.41 \times 10^{-6}$, $p = 0.046$). The strongest decreases during the task period occurred at a later time between ≈36-44 min (β ranging from -5.06×10^{-6} to -6.08×10^{-6}, all $p < 0.001$) and ≈53-60 min (β ranging from -4.63×10^{-6} to -5.49×10^{-6}, all $p < 0.003$). During the post-learning phase (≈74-127 min), all comparisons in the learning group showed significant decreases from the baseline (all $p < 0.001$). In summary, both the magnitude and the temporal persistence of MD decreases in the left middle occipital/temporal gyrus, alongside the lack of changes observed in the control group, provide strong evidence for rapid experience-dependent microstructural plasticity in the left middle occipital/temporal gyrus. This cluster also corresponds to the effects observed in

JNeurosci Accepted Manuscript

the overall linear-decrease analysis (**Fig. 4**, Table S3). The results of the post-hoc pairwise comparisons and their corresponding times are presented in Table S5.

All results from whole-brain DW-MRI and fMRI statistical analyses can be found online in the public repository NeuroVault (https://neurovault.org/collections/24041/).

Control Analyses

B0 Signal Stability. To assess whether the observed learning-related MD changes in the left middle occipital/temporal gyrus could be explained by fluctuations in b0 signal intensity, we additionally examined the temporal stability of the b0 signal. Mean b0 signal intensity was calculated for each participant by averaging across the 12 b0 images (6 AP and 6 PA directions) acquired at each time point, yielding 38 distinct time points across the experimental protocol spanning approximately 127 min. Similar to the main analyses, we used a linear mixed-effects model with time, group, scanning group, and the group × time interaction as fixed effects and participant as a random effect. The group × time interaction was not significant ($\chi^2(21) = 5.37$, $p = 1.000$), indicating no evidence for differential temporal changes in b0 signal between the learning and control groups. Consistent with this, there were no significant main effects of time ($\chi^2(37) = 12.38$, $p = 1.000$), group ($\chi^2(1) = 0.57$, $p = 0.449$), or scanning group ($\chi^2(1) = 0.04$, $p = 0.834$). Holm-corrected post-hoc comparisons of each time point with the first acquisition were also non-significant in either group (all $p = 1.000$). Thus, b0 signal intensity showed no systematic temporal or group-related variation that could account for the observed learning-related MD trajectory in the left middle occipital/temporal gyrus (**Fig. S2**).

Learning-related Changes in FA. The group × time interaction analysis on FA revealed significant increases in the learning group relative to controls in two clusters ($p_{FWE}<.05$, k=20 voxels). The first cluster (k = 60 voxels; peak MNI: [−2, −68, −32]; T = 6.66) was located in the cerebellum. The second cluster (k = 24 voxels; peak MNI: [−20, −56, 12]; T = 6.15) was located in both gray matter (%21) and white matter (%78), spanning the precuneus and the forceps

JNeurosci Accepted Manuscript

major (**Fig. 7**), a posterior callosal pathway connecting the bilateral visual cortices through the splenium (Wakana et al., 2004; Berlucchi, 2014). The voxelwise temporal overlap analysis across the 20 FA maps (t_3–t_{22}, thresholded at ≥10/20 maps) yielded a single consensus cluster (k = 15 voxels; peak MNI: [4, −39, 0]). However, this cluster was located at the midline and did not spatially overlap with either of the two clusters from the interaction analysis. The proximity to CSF-filled ventricular structures raises the possibility that partial volume effects contributed to the observed FA changes in this region (Alexander et al., 2001; Vos et al., 2011). In contrast to the robust and spatially consistent MD decreases centred on the left middle occipital/temporal gyrus, the FA increases were less spatially consistent across time points and did not co-localize with the regions showing MD interaction effects.

Correlation between Memory Performance and MD. We first used repeated-measures correlation analyses to assess the relationship between MD changes in the left middle occipital/temporal gyrus and memory performance. We would expect stronger decreases in MD to coincide with increased memory performance if learning-induced microstructural plasticity was related to behavioral performance. When memory performance was quantified using the normalized Manhattan distance, the association was negative but did not reach statistical significance (r_{rm} = -0.22, *df* = 72, *p* = 0.060). An equivalent analysis using recall accuracy yielded similar results (r_{rm} = -0.21, *df* = 72, *p* = 0.063), suggesting decreased MD with increasing memory performance, although the effects remained at the trend level.

In addition to this within-subject correlation, Pearson's correlation was used to examine the association between changes in learning-induced microstructural plasticity and memory retention (i. e., differences in memory performance between the first and fifth retrieval). No significant relationship was observed for either recall accuracy (r = -0.05, *p* = 0.63) or Manhattan distance (r = 0.10, *p* = 0.37). As a complementary approach, we performed a median split of the learning group into better- and poorer-performing subgroups based on memory retention, using both change in normalized Manhattan distance and recall accuracy

JNeurosci Accepted Manuscript

511 in retrieval performance, and compared MD change between subgroups using Welch's two-
512 sample t-tests. Neither the median split on Manhattan distance (t(68.72) = -0.72, p = .474) nor
513 the recall accuracy (t(67.39) = 0.22, p = .827) revealed a significant difference in MD change
514 between subgroups, consistent with the absence of a relationship between memory retention
515 and MD change reported above.

JNeurosci Accepted Manuscript

Discussion

We investigated the temporal dynamics of learning-induced microstructural plasticity in the human brain. Using a densely sampled DW-MRI protocol with 22 acquisitions over a 2-hour period, combined with task-based fMRI during an associative memory paradigm, we were able to assess *when* and *where* learning-induced microstructural changes occur. We found that microstructural plasticity, indexed by a decrease in MD, emerged rapidly during learning, with reductions detectable within the first ≈7 min of the task. Importantly, these MD changes continued to strengthen during the post-learning rest period, persisting for at least 2 hours. Notably, the most robust and spatially consistent effects were localized to the left middle occipital/temporal gyrus, co-localized with the functional activation.

A central finding of this study is that microstructural plasticity emerges rapidly in functionally relevant regions and persists into offline periods following the learning task. Learning-related MD reductions were observed across regions including lateral occipital cortex, precuneus, and cerebellum, consistent with the distributed circuits engaged by visuospatial learning (Brodt et al., 2016, 2018). These MD reductions did not plateau at task offset but continued to expand and persist across the post-learning rest period, with the most robust effects localized to the left middle occipital/temporal gyrus. Linear mixed-effects modelling revealed MD decreases emerging ≈7 min after learning onset and remaining detectable approximately 2 hours thereafter, consistent with prior reports demonstrating that MD changes can arise within minutes of learning (Hofstetter and Assaf, 2017; Brodt et al., 2018). Animal studies link these early changes to cellular mechanisms associated with long-term potentiation including astrocytic changes, increased BDNF expression, and elevated synaptic density (Blumenfeld-Katzir et al., 2011; Sagi et al., 2012; Garcia-Hernandez et al., 2022). Similarly, using continuous DW-MRI acquisition during learning, MD reductions have been reported to emerge within 10-30 minutes from the onset of a procedural learning and exhibit distinct temporal profiles across brain regions (Friedman et al., 2025). Extending this work, our findings

JNeurosci Accepted Manuscript

demonstrate that associative learning similarly induces microstructural changes that evolve rapidly in functionally relevant areas.

We further observed that MD decreases continued to strengthen during the post-learning rest phase, indicating that learning-related microstructural changes evolve beyond task engagement. This trajectory aligns with the systems consolidation framework (Frankland and Bontempi, 2005; Tonegawa et al., 2018), wherein newly encoded memories undergo offline reprocessing and maturation over time, particularly in neocortical areas. Consistent with this, the emergence of further microstructural changes during rest suggests that offline periods support neural and synaptic plasticity that strengthen and stabilize memory traces. Synaptic plasticity processes initiated during the task may unfold, or emerge with a delay, after learning has ended. However, because microstructural changes were already detectable within ≈7 min of learning onset, delayed processes cannot fully account for the trajectory, which spans both active learning and the subsequent rest phase.

A major aim of this project was to identify *where* in the brain learning-induced microstructural plasticity emerges most rapidly and is retained most robustly. The most consistent and spatially stable changes were evident in the left middle occipital/temporal gyrus (BA19/39). This region forms a key interface between visual perception and higher-order cognitive processing, transforming perceptual representations into increasingly abstract object- and meaning-based representations within the ventral visual stream and associated semantic networks (Patterson et al., 2007; Binder et al., 2009). It has been observed that occipito-temporal representations in visual working memory are shaped by feedback from parietal cortex (Xu, 2023), suggesting that short-term maintenance in this region might already reflect higher-order processing, potentially facilitating subsequent consolidation. It remains an open question whether such parietal-to-occipito-temporal interactions contribute to the longer-term consolidation observed here. Consistent with this account, our interaction analyses revealed MD decreases extending beyond the occipital/temporal cluster into higher-order parietal cortex, including the precuneus and adjacent posterior parietal regions. This offline parietal

JNeurosci Accepted Manuscript

engagement aligns with prior evidence that the posterior parietal cortex rapidly forms enduring memory representations within hours of learning (Brodt et al., 2018; Kleinschroth et al., 2026) and that detailed item–context learning preferentially recruits posterior parietal areas (Klinkowski et al., 2025). Together, these findings are consistent with a circuit in which higher-order parietal regions interact with occipito-temporal cortex to support the stabilization of emerging category representations. The rapid plasticity detected in occipital/temporal gyrus thus may represent an early stage of more enduring structural remodeling. Finally, the spatial correspondence between functional activation and microstructural plasticity in this region suggests that learning-engaged regions undergo structural remodeling to store memory traces within the circuits that process the corresponding sensory input, consistent with the direct neocortical encoding of category information in early visual cortex and of episodic item–context information in posterior parietal cortex (Klinkowski et al., 2025). Our findings therefore support a distributed organization in which memories form along specialized processing streams rather than exclusively in higher-order association areas.

While the middle occipital/temporal gyrus showed the most robust decreases, neither within- nor cross-subject correlations revealed a significant relationship between MD change and memory performance, consistent with previous findings (Villa et al., 2026). Learning-related MD changes, particularly if measured close to the learning experience, may thus reflect a broad signature of experience-dependent microstructural change rather than a measure that tracks individual differences in memory strength.

In addition to MD, we examined learning-related changes in FA. The interaction analysis revealed FA increases in the cerebellum and in a second cluster spanning precuneus and forceps major, a posterior callosal tract connecting bilateral visual cortices (Berlucchi, 2014), thus supporting visual communication. Both the cerebellum and precuneus contribute to visuospatial processing, including higher-order processing (Molinari and Leggio, 2007; Iglói et al., 2015; Brodt et. al., 2018). Given their roles in visuospatial processing, these FA increases may reflect training-related microstructural changes supporting visuospatial learning and

JNeurosci Accepted Manuscript

interhemispheric visual integration. However, the time-resolved overlap analysis yielded a consensus cluster near the cerebral aqueduct, where partial volume effects may produce spurious diffusion changes (Vos et al., 2011) and this cluster did not overlap with interaction results. Overall, FA effects were less spatially consistent and smaller than MD effects, providing less robust evidence of rapid experience-dependent microstructural change.

Although the control group completed very similar DW-MRI acquisitions, enabling assessment of MD changes during comparable time windows, they did not undergo the same imaging acquisition procedure as the experimental group. In particular, the learning group performed a localizer task immediately before the learning phase, which may have contributed to a cluster of surprisingly rapid MD changes observed only briefly at the very onset of learning. These early changes could reflect transient effects associated with visual stimulation, potentially linked to BOLD activity (Spencer et al., 2025), which would be expected to be most prominent during or shortly after stimulation (Hertanu et al., 2025). Importantly, however, the continued evolution of MD beyond the period of learning suggests that activity-dependent effects alone are unlikely to fully account for the temporal pattern observed here, leaving open the possibility that longer-lasting microstructural processes contribute to the later changes. Moreover, the control group did not undergo all DW-MRI measurements in the post-task period, because we considered the strain of a 3-hour wakeful task-free rest period in the MRI scanner to be hardly tolerable. This difference limits our ability to fully characterize time-dependent MD changes that may occur independently of learning, such as transient changes in water diffusion associated with neuronal activity (Tsurugizawa et al., 2013) or non-specific effects like scanner drift (Vos et al., 2017). Therefore, the apparent strengthening of MD decreases across the post-learning period should be interpreted with caution. However, the learning group showed progressive, spatially specific MD decreases in the left middle occipital/temporal gyrus during the learning phase that were absent in the control group during comparable time windows and persisted beyond active learning, providing reassurance that our findings reflect genuine learning-related microstructural plasticity rather than non-specific time-dependent,

JNeurosci Accepted Manuscript

measurement-dependent, or functional-activation-related confounds. Finally, the temporal resolution of DW-MRI is coarse compared to the sub-second timescale of synaptic plasticity processes. Nevertheless, our approach represents a substantial improvement over traditional pre-post designs. While Friedman et al. (2025) used a sliding-window approach to extract MD changes from continuously acquired DW-MRI during motor learning, our discrete acquisition strategy allowed us to synchronize 22 DW-MRI samples with task and rest phases, optimizing temporal sensitivity to state-dependent microstructural changes. Finally, fMRI and DW-MRI were acquired in an interleaved fashion rather than simultaneously, introducing temporal lags between measurements. While this prevented a continuous assessment of MD changes within participants, this design was necessary to capture functional and structural progression across the learning period. The spatial overlap between functionally active regions and sites of microstructural plasticity suggests that this limitation did not substantially impact our results. It is important to note that MD reflects mixed intra/extracellular compartments and cannot isolate dendritic complexity, synaptic density, or glial proliferation (Villa et al., 2026). Advanced DW-MRI approaches combining ultra-high-gradient protocols with SANDI can therefore help to dissociate transient cell-body expansion from sustained cell-process increases, separating plastic from non-plastic processes (Griffa et al., 2026). Such compartment-specific models may help identify which microstructural features are most affected by learning and offline consolidation.

JNeurosci Accepted Manuscript

References

Assaf Y, Johansen-Berg H, Thiebaut de Schotten M (2019). The role of diffusion MRI in neuroscience. *NMR Biomed* 32, e4050. https://doi.org/10.1002/nbm.3762.

Avants BB, Tustison NJ, Song G, Cook PA, Klein A, Gee JC (2011). A reproducible evaluation of ANTs similarity metric performance in brain image registration. *Neuroimage* 54, 2033–2044. https://doi.org/10.1016/j.neuroimage.2010.09.025.

Bakdash JZ, Marusich LR (2017). Repeated measures correlation. *Front Psychol* 8, 456. https://doi.org/10.3389/fpsyg.2017.00456.

Basser PJ, Mattiello J, LeBihan D (1994). MR diffusion tensor spectroscopy and imaging. *Biophys J* 66, 259–267. https://doi.org/10.1016/S0006-3495(94)80775-1.

Bates D, Mächler M, Bolker BM, Walker SC (2015). Fitting Linear Mixed-Effects Models Using lme4. *J Stat Softw* 67, 1–48. https://doi.org/10.18637/jss.v067.i01.

Berlucchi G (2014). Visual interhemispheric communication and callosal connections of the occipital lobes. *Cortex* 56, 1–13. https://doi.org/10.1016/j.cortex.2013.02.001.

Bihan DL (1995). Molecular diffusion, tissue microdynamics and microstructure. *NMR Biomed* 8, 375–386. https://doi.org/10.1002/nbm.1940080711.

Bihan DL (2012). Diffusion, confusion and functional MRI. *Neuroimage* 62, 1131–1136. https://doi.org/10.1016/j.neuroimage.2011.09.058.

Binder JR, Desai RH, Graves WW, Conant LL (2009). Where Is the Semantic System? A Critical Review and Meta-Analysis of 120 Functional Neuroimaging Studies. *Cereb Cortex* 19, 2767–2796. https://doi.org/10.1093/cercor/bhp055.

Blumenfeld-Katzir T, Pasternak O, Dagan M, Assaf Y (2011). Diffusion MRI of structural brain plasticity induced by a learning and memory task. *PLoS One* 6, e20678. https://doi.org/10.1371/journal.pone.0020678.

Brodt S, Gais S (2021). Memory Engrams in the Neocortex. *Neuroscientist* 27, 427–444. https://doi.org/10.1177/1073858420941528.

Brodt S, Gais S, Beck J, Erb M, Scheffler K, Schönauer M (2018). Fast track to the neocortex: A memory engram in the posterior parietal cortex. *Science* 362, 1045–1048. https://doi.org/10.1126/science.aau2528.

Brodt S, Pöhlchen D, Flanagin VL, Glasauer S, Gais S, Schönauer M (2016). Rapid and independent memory formation in the parietal cortex. *Proc Natl Acad Sci U S A* 113, 13251–13256. https://doi.org/10.1073/pnas.1605719113.

Callow DD, Kommula Y, Stark CEL, Smith JC (2023). Acute cycling exercise and hippocampal subfield function and microstructure in healthy older adults. *Hippocampus* 33, 1123–1138. https://doi.org/10.1002/hipo.23571.

Darquié A, Poline JB, Poupon C, Saint-Jalmes H, Le Bihan D (2001). Transient decrease in water diffusion observed in human occipital cortex during visual stimulation. *Proc Natl Acad Sci U S A* 98, 9391–9395. https://doi.org/10.1073/pnas.151125698.

JNeurosci Accepted Manuscript

682 Draganski B, Gaser C, Busch V, Schuierer G, Bogdahn U, May A (2004). Changes in
683 grey matter induced by training. *Nature* 427, 311–312.
684 https://doi.org/10.1038/427311a.

685 Esteban O et al. (2020). Analysis of task-based functional MRI data preprocessed with
686 fMRIPrep. *Nat Protoc* 15, 2186–2202. https://doi.org/10.1038/s41596-020-0327-
687 3.

688 Frankland PW, Bontempi B (2005). The organization of recent and remote memories.
689 *Nat Rev Neurosci* 6, 119–130. https://doi.org/10.1038/nrn1607.

690 Friedman N, Malovani C, Perets I, Kenin E, Bernstein-Eliav M, Tavor I (2025). Continuous
691 Diffusion-Detected Neuroplasticity during Motor Learning. *J Neurosci* 45, e0537.
692 https://doi.org/10.1523/JNEUROSCI.1152-24.2025.

693 Garcia-Hernandez R, Cerdán Cerdá A, Trouve Carpena A, Drakesmith M, Koller K, Jones
694 DK, Canals S, De Santis S (2022). Mapping microglia and astrocyte activation in
695 vivo using diffusion MRI. *Sci Adv* 8, eabj8378.
696 https://doi.org/10.1126/sciadv.abq2923.

697 Gorgolewski K, Burns CD, Madison C, Clark D, Halchenko YO, Waskom ML, Ghosh SS
698 (2011). Nipype: A Flexible, Lightweight and Extensible Neuroimaging Data
699 Processing Framework in Python. *Front Neuroinform* 5, 13.
700 https://doi.org/10.3389/fninf.2011.00013.

701 Gorgolewski KJ et al. (2016). The brain imaging data structure, a format for organizing
702 and describing outputs of neuroimaging experiments. *Sci Data* 3, 160044.
703 https://doi.org/10.1038/sdata.2016.44.

704 Griffa G, Deleglise A, Solano A, Jacobacci F, De Pino G, Della-Maggiore V (2024). The
705 human hippocampus is involved in implicit motor learning. *bioRxiv*.
706 https://doi.org/10.1101/2024.08.30.610548.

707 Griffa G, Palombo M, Yeffal A, Lee H-H, Solano A, Huang SY, Della-Maggiore V (2026).
708 Learning engages transient and sustained cellular mechanisms in the human
709 brain. *PLoS Biol* 24, e3003861. https://doi.org/10.1371/journal.pbio.3003861.

710 Hebscher M, Wing E, Ryan J, Gilboa A (2019). Rapid Cortical Plasticity Supports Long-
711 Term Memory Formation. *Trends Cogn Sci* 23, 989–1002.
712 https://doi.org/10.1016/j.tics.2019.09.009.

713 Hertanu A, Pavan T, Jelescu IO (2025). Somatosensory-evoked response induces
714 extensive diffusivity and kurtosis changes associated with neural activity in
715 rodents. *Imaging Neurosci* 3, e00445. https://doi.org/10.1162/imag_a_00445.

716 Hofstetter S, Assaf Y (2017). The rapid development of structural plasticity through short
717 water maze training: A DTI study. *Neuroimage* 155, 202–208.
718 https://doi.org/10.1016/j.neuroimage.2017.04.056.

719 Hofstetter S, Friedmann N, Assaf Y (2017). Rapid language-related plasticity:
720 microstructural changes in the cortex after a short session of new word learning.
721 *Brain Struct Funct* 222, 1231–1241. https://doi.org/10.1007/s00429-016-1273-2.

JNeurosci Accepted Manuscript

Hua K, Zhang J, Wakana S, Jiang H, Li X, Reich DS, Calabresi PA, Pekar JJ, van Zijl PCM, Mori S (2008). Tract probability maps in stereotaxic spaces: Analyses of white matter anatomy and tract-specific quantification. *Neuroimage* 39, 336–347. https://doi.org/10.1016/j.neuroimage.2007.07.053.

Iglói K, Doeller CF, Paradis AL, Benchenane K, Berthoz A, Burgess N, Rondi-Reig L (2015). Interaction Between Hippocampus and Cerebellum Crus I in Sequence-Based but not Place-Based Navigation. *Cereb Cortex* 25, 4146–4154. https://doi.org/10.1093/cercor/bhu132.

Jacobacci F, Armony JL, Yeffal A, Lerner G, Amaro E, Jovicich J, Doyone J, Della-Maggiore V (2020). Rapid hippocampal plasticity supports motor sequence learning. *Proc Natl Acad Sci U S A* 117, 23898–23903. https://doi.org/10.1073/pnas.2009576117.

Jenkinson M, Beckmann CF, Behrens TEJ, Woolrich MW, Smith SM (2012). FSL. *Neuroimage* 62, 782–790. https://doi.org/10.1016/j.neuroimage.2011.09.015.

Johansen-Berg H, Baptista CS, Thomas AG (2012). Human Structural Plasticity at Record Speed. *Neuron* 73, 1058–1060. https://doi.org/10.1016/j.neuron.2012.03.001.

Keller TA, Just MA (2016). Structural and functional neuroplasticity in human learning of spatial routes. *Neuroimage* 125, 256–266. https://doi.org/10.1016/j.neuroimage.2015.10.015.

Kleinschroth F, Villa S, Lenders A, Brodt S, Gais S, Schönauer M, Kumral D (2026). Rapid expansion and renormalization of parietal gray matter volume following associative learning. *bioRxiv*. https://doi.org/10.64898/2026.04.30.721879.

Klinkowski S, Seewald A, Fath B, Kasties V, Iliopoulos P, Schmidt S, Voss F, Erb M, Scheffler K, Gais S, Brodt S (2025). Direct encoding of new visual concepts in early visual cortex. *bioRxiv*. https://doi.org/10.1101/2025.10.07.680862.

Klinzing JG, Niethard N, Born J (2019). Mechanisms of systems memory consolidation during sleep. *Nat Neurosci* 22, 1598–1610. https://doi.org/10.1038/s41593-019-0467-3.

Lenth RV, Piaskowski J (2017). emmeans: Estimated Marginal Means, aka Least-Squares Means. R package version 1.1. Retrieved from https://CRAN.R-project.org/package=emmeans.

McClelland JL, McNaughton BL, O'Reilly RC (1995). Why there are complementary learning systems in the hippocampus and neocortex: Insights from the successes and failures of connectionist models of learning and memory. *Psychol Rev* 102, 419–457. https://doi.org/10.1037/0033-295X.102.3.419.

Molinari M, Leggio MG (2007). Cerebellar information processing and visuospatial functions. *Cerebellum* 6, 214–220. https://doi.org/10.1080/14734220701230870.

Mori S, Oishi K, Jiang H, Jiang L, Li X, Akhter K, Hua K, Faria AV, Mahmood A, Woods R, Toga AW, Pike GB, Neto PR, Evans A, Zhang J, Huang H, Miller MI, van Zijl P, Mazziotta J (2008). Stereotaxic white matter atlas based on diffusion tensor

JNeurosci Accepted Manuscript

763 imaging in an ICBM template. *Neuroimage* 40, 570–582.
764 https://doi.org/10.1016/j.neuroimage.2007.12.035.

765 Patterson K, Nestor PJ, Rogers TT (2007). Where do you know what you know? The
766 representation of semantic knowledge in the human brain. *Nat Rev Neurosci* 8,
767 976–987. https://doi.org/10.1038/nrn2277.

768 Sagi Y, Tavor I, Hofstetter S, Tzur-Moryosef S, Blumenfeld-Katzir T, Assaf Y (2012).
769 Learning in the Fast Lane: New Insights into Neuroplasticity. *Neuron* 73, 1195–
770 1203. https://doi.org/10.1016/j.neuron.2012.01.025.

771 Scholz J, Klein MC, Behrens TEJ, Johansen-Berg H (2009). Training induces changes
772 in white-matter architecture. *Nat Neurosci* 12, 1370–1371.
773 https://doi.org/10.1038/nn.2412.

774 Spencer APC, Nguyen-Duc J, de Riedmatten I, Szczepankiewicz F, Jelescu IO (2025).
775 Mapping grey and white matter activity in the human brain with isotropic ADC-
776 fMRI. *Nat Commun* 16, 5036. https://doi.org/10.1038/s41467-025-60357-5.

777 Stark CEL, Squire LR (2001). When zero is not zero: The problem of ambiguous baseline
778 conditions in fMRI. *Proc Natl Acad Sci U S A* 98, 12760–12766.
779 https://doi.org/10.1073/pnas.221462998.

780 Stee W, Legouhy A, Guerreri M, Villemonteix T, Zhang H, Peigneux P (2023).
781 Microstructural dynamics of motor learning and sleep-dependent consolidation: A
782 diffusion imaging study. *iScience* 26, 108426.
783 https://doi.org/10.1016/j.isci.2023.108426.

784 Tavor I, Botvinik-Nezer R, Bernstein-Eliav M, Tsarfaty G, Assaf Y (2020). Short-term
785 plasticity following motor sequence learning revealed by diffusion magnetic
786 resonance imaging. *Hum Brain Mapp* 41, 442–452.
787 https://doi.org/10.1002/hbm.24814.

788 Tavor I, Hofstetter S, Assaf Y (2013). Micro-structural assessment of short term plasticity
789 dynamics. *Neuroimage* 81, 1–7.
790 https://doi.org/10.1016/j.neuroimage.2013.05.050.

791 Tonegawa S, Morrissey MD, Kitamura T (2018). The role of engram cells in the systems
792 consolidation of memory. *Nat Rev Neurosci* 19, 485–498.
793 https://doi.org/10.1038/s41583-018-0031-2.

794 Tsurugizawa T, Ciobanu L, Bihan DL (2013). Water diffusion in brain cortex closely tracks
795 underlying neuronal activity. *Proc Natl Acad Sci U S A* 110, 11636–11641.
796 https://doi.org/10.1073/pnas.1303178110.

797 Villa S, Kleinschroth F, Schönauer M, Kumral D (2026). Experience-dependent rapid
798 structural changes in the human brain: A systematic review. *Neurosci Biobehav*
799 *Rev* 187, 106736. https://doi.org/10.1016/j.neubiorev.2026.106736.

800 Vos SB, Jones DK, Viergever MA, Leemans A (2011). Partial volume effect as a hidden
801 covariate in DTI analyses. *Neuroimage* 55, 1566–1576.
802 https://doi.org/10.1016/j.neuroimage.2011.01.048.

JNeurosci Accepted Manuscript

803 Vos SB, Tax CMW, Luijten PR, Ourselin S, Leemans A, Froeling M (2017). The
804 importance of correcting for signal drift in diffusion MRI. *Magn Reson Med* 77,
805 285–299. https://doi.org/10.1002/mrm.26124.

806 Wakana S, Jiang H, Nagae-Poetscher LM, Van Zijl PCM, Mori S (2004). Fiber Tract–
807 based Atlas of Human White Matter Anatomy. *Radiology* 230, 77–87.
808 https://doi.org/10.1148/radiol.2301021640.

809 Xu Y (2023). Parietal-driven visual working memory representation in occipito-temporal
810 cortex. *Curr Biol* 33, 4516–4523.e5. https://doi.org/10.1016/j.cub.2023.08.080

811 Zatorre RJ, Fields RD, Johansen-Berg H (2012). Plasticity in gray and white:
812 neuroimaging changes in brain structure during learning. *Nat Neurosci* 15, 528–
813 536. https://doi.org/10.1038/nn.3045.

814

JNeurosci Accepted Manuscript

Fig. 1. Experimental timeline and imaging protocol. Both scanning groups (A and B) underwent baseline MRI acquisitions, including T1-weighted (T1-w) and T2-weighted (T2-w) scans, followed by an image-location learning task consisting of alternating encoding (E) and retrieval (R) blocks (total duration: 60 min), with interleaved task-based fMRI and diffusion-weighted MRI (DW-MRI) acquisitions. After a short break (15 min), post-task resting-state fMRI and DW-MRI data were acquired (55 min), followed by a final T1-weighted scan. In total, 22 DW-MRI scans were acquired across baseline, task, and post-learning periods for more than 2 hours, enabling characterization of temporal dynamics of learning-induced microstructural changes in the brain. In the control condition, after identical baseline scans, participants remained at rest during the period corresponding to the learning task while interleaved resting-state fMRI and DW-MRI were acquired. Following a 90-min break, additional DW-MRI acquisitions and a final T1-w scans were measured. The control group completed 14 DW-MRI scans across comparable time windows.

JNeurosci Accepted Manuscript

828 **Fig. 2. Schematic depiction of encoding and retrieval trials in the image-location task.**
829 Participants learned and recalled image-location associations across four encoding-retrieval
830 repetitions. **A.** During encoding, 28 image pairs were presented in a random order, with each
831 image assigned to a unique position on a 7×4 grid and shown once as the first item and once
832 as the second item. **B.** During retrieval, the first image cued the recall of its pair and
833 participants indicated the location of the associated image using a button-controlled cursor.

834

JNeurosci Accepted Manuscript

Fig. 3. Behavioral performance and functional activity. Violin plots show the distribution of individual participant data for each run, while boxplots indicate the median and interquartile range, and dots represent individual participants. **A.** Percentage of correct responses increased across repetitions, while **B.** Manhattan Distance (normalized) decreased, indicating better recall accuracy. Repeated-measures ANOVAs revealed a significant effect of repetition on both measures (p<0.001). **C.** Statistical parametric maps illustrating general encoding-related activity (yellow–orange) and retrieval-related activity (blue–purple). **D**. Joint inference across task-based fMRI (encoding and retrieval) and the overlap map of Mean Diffusivity (MD) changes (each session [t_3–t_{22}] relative to baseline [t_1]) revealed a shared cluster in the left middle occipital/temporal gyrus (dark pink; x = −41, y = −72, z = 21). Of the 17 voxels showing consistent MD change across time, 14 also overlapped with task-based functional activation, indicating that learning-related functional activity was accompanied by microstructural plasticity.

JNeurosci Accepted Manuscript

Fig. 4. Learning-specific linear decreases in mean diffusivity (MD) across 22 sessions. We computed a group × time interaction (learning vs. control) using a whole-brain flexible factorial analysis with a linear decrease contrast. Relative to control, we found decreased MD in the learning group in several brain regions including the middle occipital-temporal gyrus, cerebellum, precuneus, superior parietal lobule, precentral gyrus, postcentral gyrus, cuneal cortex, angular gyrus, and lingual gyrus. Thresholded at $p < 0.05$, FWE-corrected with a minimum cluster size of k = 20 voxels.

JNeurosci Accepted Manuscript

Fig. 5. Temporal trajectories of learning-induced microstructural changes in the whole brain across sessions. We examined learning-induced changes in mean diffusivity (MD) at the whole-brain level by comparing baseline MD (t_1) with each subsequent time point (t_2–t_{22}), relative to the control group, yielding 21 contrasts. Results revealed a progressive reduction in MD across several regions, including the precuneus, middle occipital/temporal gyrus, cerebellum, and lateral occipital cortex. Time points t_1–t_2 were defined as baseline, t_3–t_{10} as the learning phase, and t_{11}–t_{22} as the post-learning phase. All statistical parametric maps were thresholded at $p < 0.001$ (uncorrected) with a minimum cluster size of k = 20 voxels.

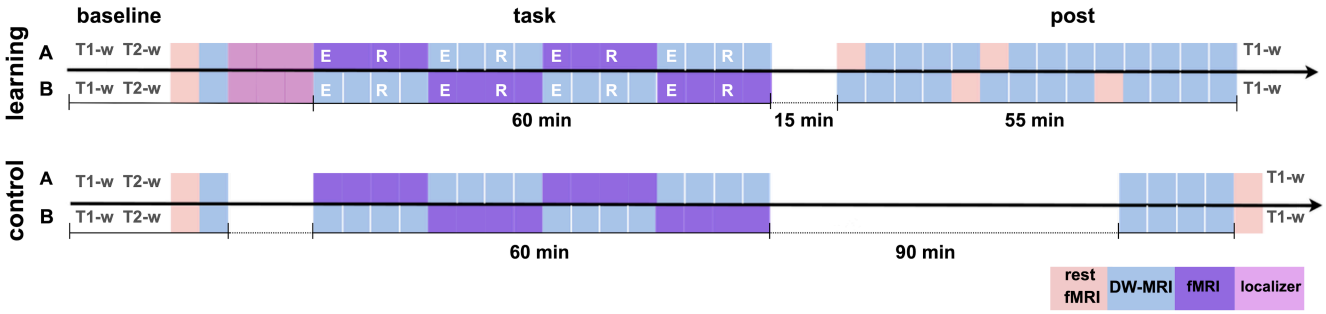
JNeurosci Accepted Manuscript

Fig. 6. Fine-grained temporal dynamics of microstructural changes in left middle occipital/temporal gyrus. Mean Diffusivity (MD) changes from the baseline, expressed as percentage. Each dot represents an MD change of each individual from their baseline (-20 min), while bar plots show the distribution of percentage changes at each time point. The post-hoc results from the linear mixed effect model indicate that the learning group demonstrates consistent MD decreases in the left middle occipital/temporal gyrus that emerge during early task phases and persist throughout the post-learning period, while the control group shows minimal deviation from baseline across all time points. For visualization purposes, outliers (N_{img}=43 out of 2146) were removed using the interquartile range method, while all statistical analyses were performed on the complete data points (N_{img}=2146).

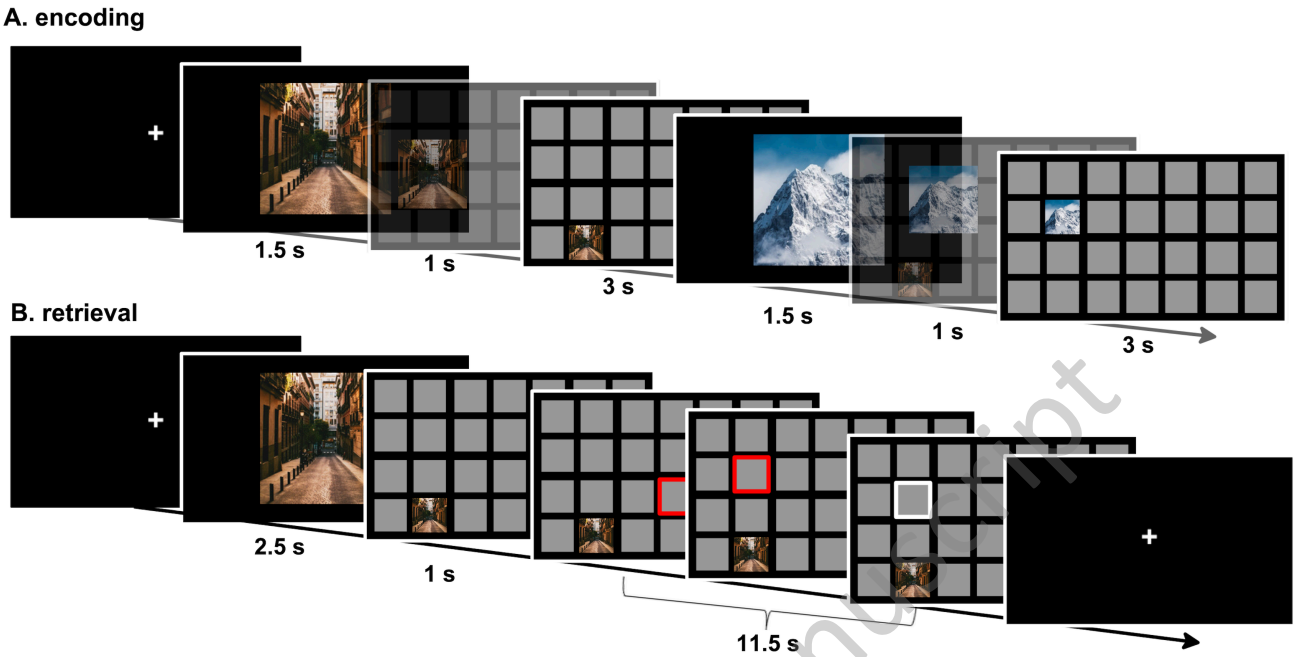
JNeurosci Accepted Manuscript

Fig. 7. Learning-specific linear increases in fractional anisotropy (FA) across 22 sessions. We computed a group × time interaction (learning vs. control) using a whole-brain flexible factorial analysis with a linear increase contrast. Relative to control, we found increase FA in the learning group in two brain clusters: cerebellum and another cluster spanning the precuneus and forceps major. Thresholded at $p < 0.05$, FWE-corrected with a minimum cluster size of k = 20 voxels.

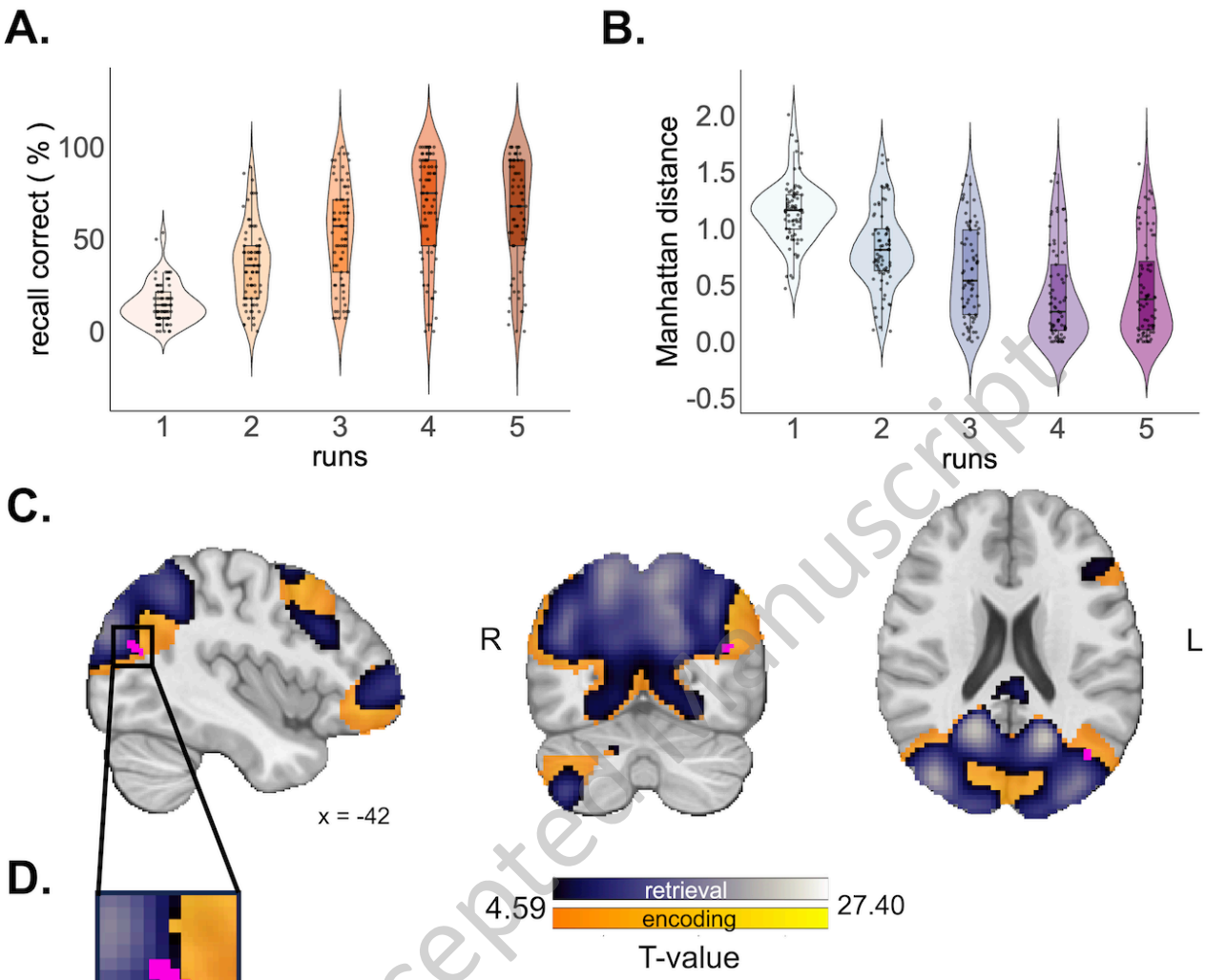
JNeurosci Accepted Manuscript



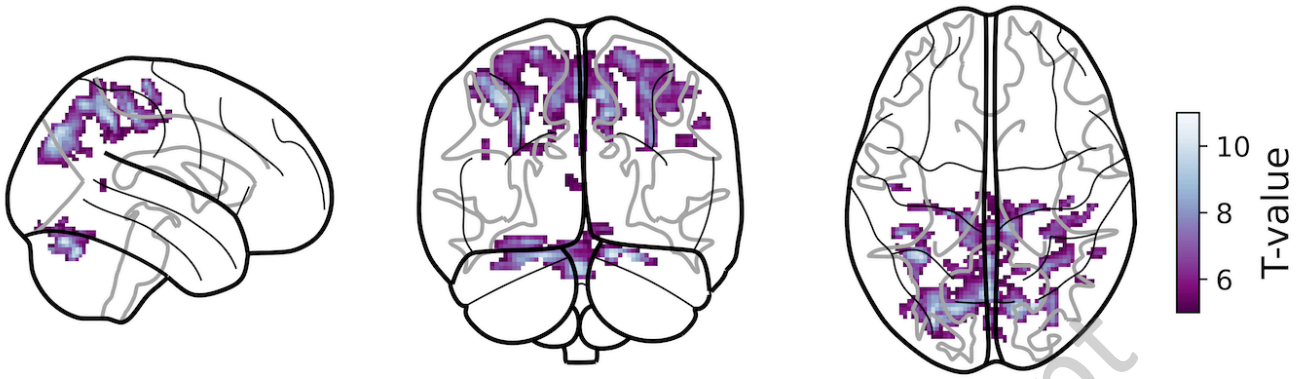
JNeurosci Accepted Manuscript



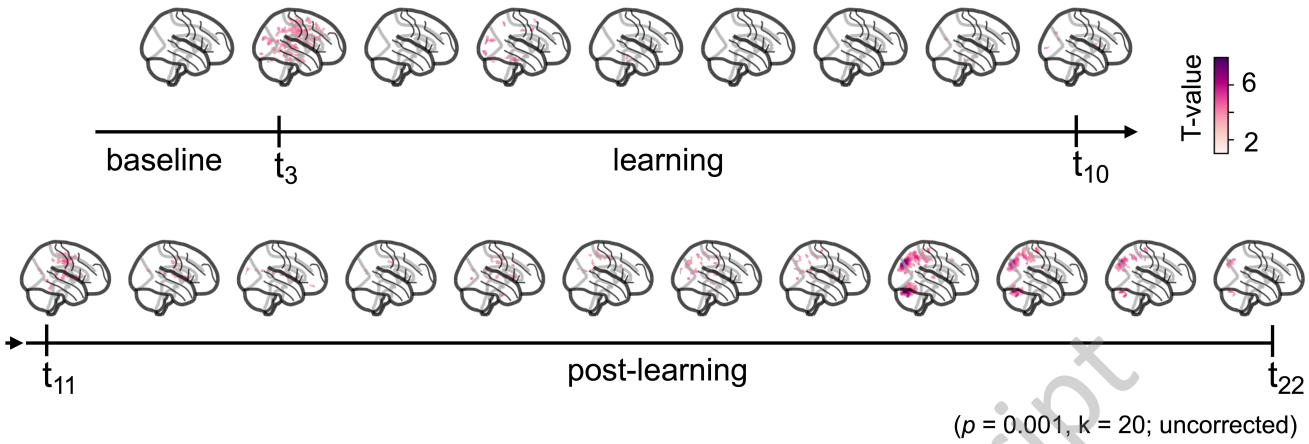
JNeurosci Accepted Manuscript



JNeurosci Accepted Manuscript

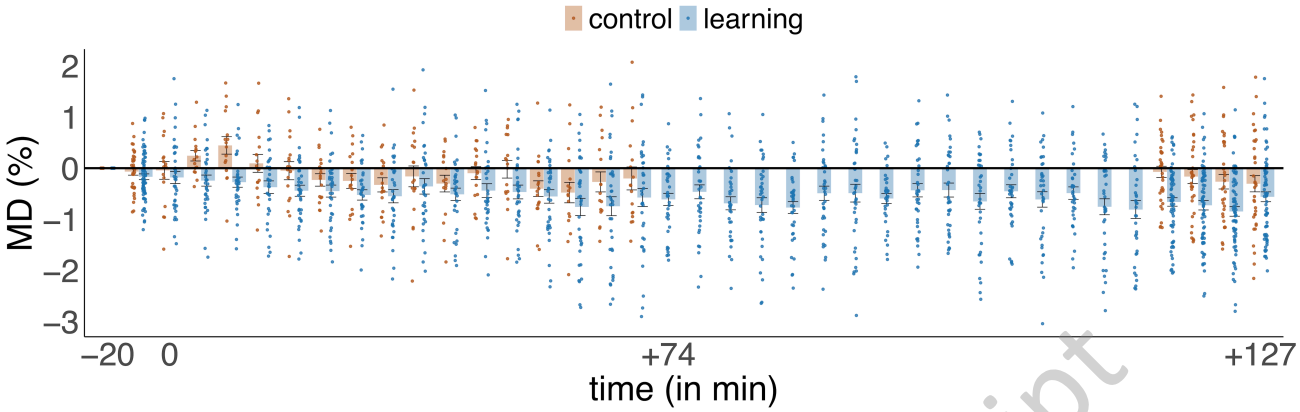


JNeurosci Accepted Manuscript

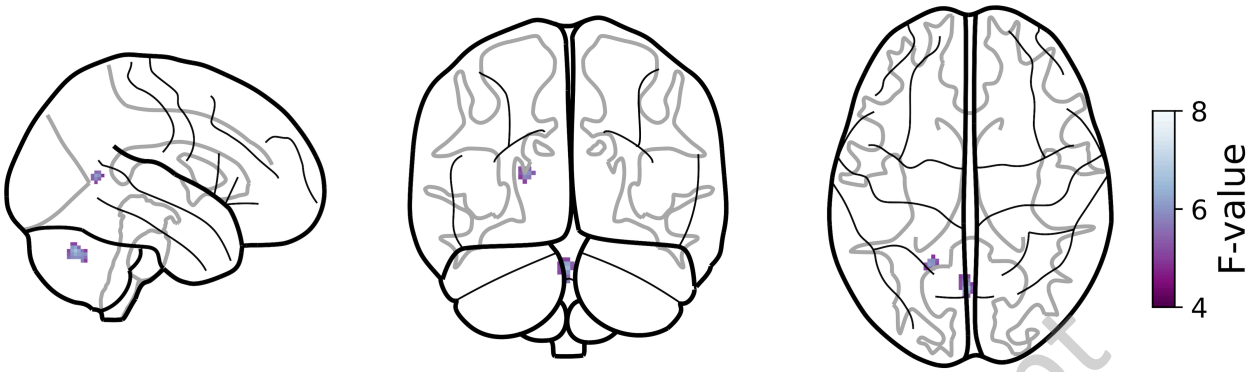


(p = 0.001, k = 20; uncorrected)

JNeurosci Accepted Manuscript



JNeurosci Accepted Manuscript



JNeurosci Accepted Manuscript